

Effect of Energy Polydispersity on the Nature of Lennard-Jones Liquids

Trond S. Ingebrigtsen^{1,*} and Hajime Tanaka^{1,†}

¹*Institute of Industrial Science, University of Tokyo,
4-6-1 Komaba, Meguro-ku, Tokyo 153-8505, Japan*

(Dated: June 3, 2016)

In the companion paper [T. S. Ingebrigtsen and H. Tanaka, J. Phys. Chem. B 119, 11052 (2015)] the effect of size polydispersity on the nature of Lennard-Jones (LJ) liquids, which represent most molecular liquids without hydrogen bonds, was studied. More specifically, it was shown that even highly size polydisperse LJ liquids are Roskilde-simple (RS) liquids. RS liquids are liquids with strong correlation between constant volume equilibrium fluctuations of virial and potential energy and are simpler than other types of liquids. Moreover, it was shown that size polydisperse LJ liquids have isomorphs to a good approximation. Isomorphs are curves in the phase diagram of RS liquids along which structure, dynamics, and some thermodynamic quantities are invariant in dimensionless (reduced) units. In this paper, we study the effect of energy polydispersity on the nature of LJ liquids. We show that energy polydisperse LJ liquids are RS liquids. However, a tendency of particle segregation which increases with the degree of polydispersity leads to a loss of strong virial-potential energy correlation, but is mitigated with increasing temperature and/or density. Isomorphs are a good approximation also for energy polydisperse LJ liquids, although particle-resolved quantities display a somewhat poorer scaling compared to the mean quantities along the isomorph.

I. INTRODUCTION

Fluids showing a dispersion in a variable characterizing the constituent molecules are called polydisperse fluids^{1,2}. The dispersed variable could be the size of the molecules, but also their shape, charge, and more. A binary mixture comprised of two different molecular sizes is a simple example of a polydisperse fluid. However, in general the fluid can consist of numerous components. Bitumen is an example of a highly dispersed fluid with millions of components and constitutes the “glue” part of asphalt owing to the unique and perplexing properties obtained from the highly polydisperse and viscous mixture³.

Polydisperse fluids are interesting from both a theoretical and an experimental perspective^{4–25}. In experiments, for instance, polydispersity can be used as a tool to avoid crystallization and thus facilitate the study of highly viscous fluids^{21,26}. The reason for the latter is the higher nucleation barriers of the supercooled polydisperse fluid²² due to the increase of frustration against crystallization^{27,28}. Theoretically, polydisperse fluids pose a challenge as new perplexing phenomena, e.g., fractionation^{8,9,12,14,15} can occur. Fractionation is the phenomenon that takes place when the fluid (or solid) forms additional phases, each showing a unique distribution. In fact, describing this phenomenon correctly has led to the creation of new theories as well as new simulation methods^{9,12,14,15,29}.

In a recent paper³⁰ we studied the effect of size polydispersity on the property of being a so-called Roskilde-simple (RS) liquid^{31–37}. RS liquids are characterized by having strong correlations between virial W and potential energy U equilibrium fluctuations at constant volume V . The virial-potential energy correlation is quantified

via the correlation coefficient R given by

$$R = \frac{\langle \Delta W \Delta U \rangle}{\sqrt{\langle (\Delta W)^2 \rangle} \sqrt{\langle (\Delta U)^2 \rangle}}, \quad (1)$$

in which Δ denotes deviation from the mean values, $\langle \dots \rangle$ provides NVT ensemble averages, and $-1 \leq R \leq 1$. RS liquids are defined pragmatically³² by requiring $R \geq 0.90$ and R depends on the state point.

The class of RS liquids is believed to include most or all van der Waals and metallic liquids, but to exclude most or all covalent-bonding, hydrogen-bonding, strongly ionic, and dipolar liquids^{32,37}. RS liquids are simpler than other types of liquids displaying, e.g., isomorphs^{35,38}. Isomorphs are curves in the phase diagram of RS liquids along which structure, dynamics, and some thermodynamic quantities are invariant in dimensionless (reduced) units; reduced units refer in this case to macroscopic quantities, such as T and $\rho^{-1/3}$, rather than the usual approach in simulations via microscopic quantities (see Ref. 35 for details).

In the companion paper³⁰, we demonstrated that even highly size polydisperse Lennard-Jones (LJ) liquids are RS liquids. Furthermore, it was shown that these liquids have isomorphs to a good approximation. Experimental liquids, however, are often dispersed in additional variables besides their size. As an example: Colloidal fluids can have distribution in their size as well as their charge³⁹; polymer fluids need both a size and energy distribution to be described correctly in simulations⁴⁰. In this paper we study energy polydisperse LJ liquids as a first step in understanding how these additional factors affect polydisperse RS liquids. In experiments, a polydispersity in the refractive index of the particles should provide a similar situation.

An energy distribution has in previous studies been applied together with, e.g., a distribution in the molecular size^{12,40}, and only very recently been studied isolated for its interesting phase behavior^{41–43}. To fully unravel the relative effects of polydispersity on strong virial-potential energy correlation we focus, in this study, on energy polydisperse LJ liquids⁴¹. Although this system is less experimentally realizable than size polydisperse systems, we believe that the conclusions drawn from this kind of study are necessary for understanding the effect of polydispersity on the nature of LJ liquids.

The paper is organized as follows. Simulation and model details are presented in Sec. II. Section III provides a brief introduction to RS liquids and their simple properties. Section IV presents molecular dynamics (MD) computer simulation results. Finally, Sec. V summarizes the paper and provides a brief outlook.

II. SIMULATION AND MODEL DETAILS

MD computer simulations are utilized to investigate the effect of energy polydispersity on strong virial-potential energy correlation in the NVT ensemble⁴⁴. The RUMD package⁴⁵ is used to simulate highly-efficient GPU MD. A system size of $N = 131072$ particles is used in the current study, and finite-size effects were checked by simulating $N = 62500$ and $N = 5000$ particles at selected state points. Finite-size effects were observed only for the $N = 5000$ system at very high polydispersities.

The energy polydisperse LJ liquid has pair potential

$$v_{ij}(r) = 4\epsilon_{ij} \left[\left(\frac{\sigma}{r} \right)^{12} - \left(\frac{\sigma}{r} \right)^6 \right], \quad (2)$$

and total potential energy function $U \equiv \sum_{i<j} v_{ij}(r)$. In Eq. (2): σ and ϵ_{ij} set, respectively, the length and energy scale of the pair interaction between particle i and particle j ($i, j = 1, \dots, N$). The pair interaction energy ϵ_{ij} is assigned according to the rule^{41,46}

$$\epsilon_{ij} = \sqrt{\epsilon_i \epsilon_j}. \quad (3)$$

The distributed variables ϵ_i and ϵ_j are chosen from a uniform distribution (i.e., a flat distribution) on the interval from ϵ^{min} to ϵ^{max} . The units of the simulation are defined by setting the mean values over the N particles to unity, i.e., $\sigma_{\bar{N}\bar{N}} = 1$, $\epsilon_{\bar{N}\bar{N}} = 1$, $m_{\bar{N}} = 1$. A truncated-and-shifted pair potential cutoff at $r_c = 2.5\sigma$ is applied. We follow the standard approach in the literature and define the dimensionless polydispersity index δ as the ratio of the distributed variable's standard deviation and mean¹⁷. Polydispersities are studied in the interval from $\delta = 0\%$ to $\delta = 51.92\%$.

Furthermore, but in lesser detail, we study a modified version of the energy polydisperse LJ liquid in which the repulsive force is identical to that of a single-component

LJ liquid, i.e., the repulsive force is not modified by the energy polydispersity. The pair potential is given by

$$v_{ij}^{att}(r) = v_{ij}(r)/\epsilon_{ij} + (1 - \epsilon_{ij}), \quad r < 2^{1/6}\sigma, \quad (4)$$

$$v_{ij}^{att}(r) = v_{ij}(r), \quad r \geq 2^{1/6}\sigma. \quad (5)$$

Figure 1 displays the range of pair potentials for these two systems with $\delta = 51.92\%$ (i.e., $\epsilon^{min} = 0.1$ and $\epsilon^{max} = 1.9$). The motivation for studying the latter system is that Eq. (2), by modifying the repulsive force, also introduces a size polydispersity into the system at very high polydispersities (see the black curve in Fig. 1(a)).

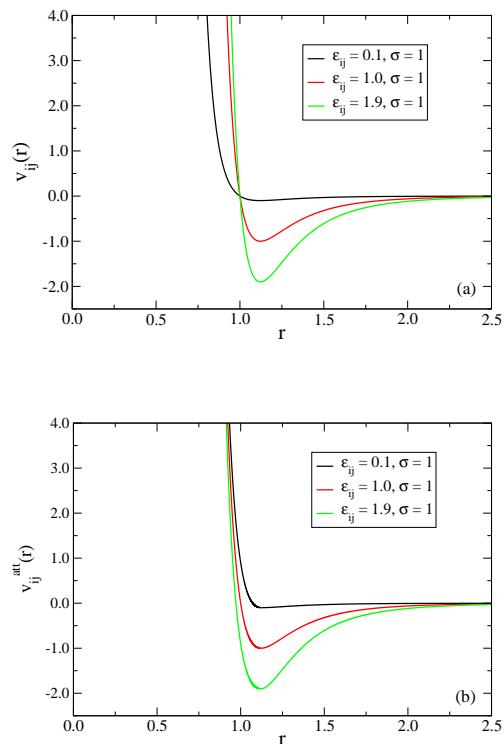


FIG. 1: The range of pair potentials for energy polydisperse LJ liquids with $\delta = 51.92\%$ (i.e., $\epsilon^{min} = 0.1$ and $\epsilon^{max} = 1.9$). (a) Pair potentials of Eq. (2). (b) Pair potentials of Eqs. (4)-(5) in which the repulsive force is identical to that of a single-component LJ liquid.

III. ROSKILDE-SIMPLE LIQUIDS

This section provides a brief introduction to RS liquids and their associated simple properties^{31–37}. A more detailed review is given in Ref. 47. RS liquids were initially known as strongly-correlating liquids, but due to the confusion with strongly-correlated electron systems the name was changed in 2011 to RS liquids³⁷. RS liquids are defined via the correlation coefficient

$$R = \frac{\langle \Delta W \Delta U \rangle}{\sqrt{\langle (\Delta W)^2 \rangle} \sqrt{\langle (\Delta U)^2 \rangle}}, \quad (6)$$

to be whenever $R \geq 0.90$. R varies throughout the phase diagram for a given liquid, but is usually observed to be high in most of the liquid part of the phase diagram for a RS liquid. In fact, strong correlation is also observed in the crystal phase showing higher correlation coefficients than in the liquid⁴⁸. Inverse power-law fluids interacting via r^{-n} pair potentials are perfectly correlating with $R = 1$ since $\Delta W = (n/3)\Delta U$.

Model systems identified to belong to RS liquids^{31–33,49–51} include the standard single-component LJ liquid, the Kob-Andersen binary LJ mixture⁵², the asymmetric dumbbell model⁵¹, the Lewis-Wahnström OTP model⁵³, and many more. Strong correlation has also been experimentally verified for several van der Waals liquids^{54–56}.

RS liquids are characterized by having isomorphs in the phase diagram^{35,38}. Consider two state points in a liquid's phase diagram with density and temperature (ρ_1, T_1) and (ρ_2, T_2) . These two state points are defined to be isomorphic if the following holds: Whenever micro-configurations of state point (1) and of state point (2) have the same reduced coordinates (\mathbf{R} is a $3N$ -dimensional configurational-space vector and $\rho \equiv N/V$),

$$\rho_1^{1/3} \mathbf{R}^{(1)} = \rho_2^{1/3} \mathbf{R}^{(2)}, \quad (7)$$

these two configurations have proportional Boltzmann factors, i.e.,

$$e^{-U(\mathbf{R}^{(1)})/k_B T_1} = C_{12} e^{-U(\mathbf{R}^{(2)})/k_B T_2}. \quad (8)$$

An isomorph is then defined as a continuous curve of state points for which all state points are pairwise isomorphic. C_{12} is a constant and depends only on the state points (1) and (2), but not on their micro-configurations. Invariants along the isomorph include the structure and dynamics in dimensionless (reduced) units, but also several thermodynamics quantities such as the excess entropy $s_{ex} \equiv S_{ex}/N$ (with respect to an ideal gas).

RS liquids are simpler than other types of liquids^{37,57}. Temperature, for example, factors⁵⁷ into a product of a function of density and a function of excess entropy

$$T = h(\rho) f(s_{ex}). \quad (9)$$

The function $h(\rho)$ inherits the analytical structure of the potential energy function⁵⁷ and can be used to generate isomorphs in simulations by keeping $h(\rho)/T$ constant since s_{ex} is constant along an isomorph (see also Eq. (11) in the next section). Previous investigations have also detailed that RS liquids and isomorphs are

relevant for nanoconfined liquids^{58,59}, out-of-equilibrium liquids⁶⁰, polymer fluids⁶¹, crystals⁴⁸, and more.

Recently, the concept of isomorphs was reformulated⁶². The isomorphic condition now reads

$$U(\mathbf{R}_a) < U(\mathbf{R}_b) \Rightarrow U(\lambda \mathbf{R}_a) < U(\lambda \mathbf{R}_b), \quad (10)$$

where λ is a scalar, and \mathbf{R}_a and \mathbf{R}_b are two different micro-configurations of a chosen state point. This definition encapsulates the previous definition of isomorphs (Eq. (8)) as a first-order approximation⁶². Although the reformulation is a minor correction of the isomorph theory, it has the consequence that the constant-volume heat capacity is not (formally) invariant along an isomorph^{35,62}.

IV. RESULTS

In this section we study energy polydisperse LJ liquids by varying the degree of polydispersity δ . The effect of polydispersity on strong virial-potential correlation is studied first and subsequently isomorphs of energy polydisperse LJ liquids are investigated.

A. Virial-potential energy correlation

The correlation coefficient R and density-scaling exponent⁵⁷ $\gamma \equiv \langle \Delta U \Delta W \rangle / \langle (\Delta U)^2 \rangle$ are presented in Fig. 2 as functions of polydispersity δ for the energy polydisperse LJ system (Eq. (2)). The following state points are studied in the figure:

1. Three different temperatures $T = 0.70, 1.00, 4.00$ with $\rho = 0.85$ (black curves). These state points correspond to a path from the triple point into the fluid region at $\delta = 0\%$.
2. A state point with $\rho = 0.95$ and $T = 1.50$ (red curve). This state point is located close to the freezing line at $\delta = 0\%$.
3. A state point with $\rho = 1.10$ and $T = 0.70$ (blue curve). A perfect FCC lattice was prepared, a random (energy) distribution in space introduced, and the crystal simulated.

Each of the black curves displays a weakening of the strong virial-potential energy correlation with increasing polydispersity (Fig. 2(a)). In fact, the curve at $T = 0.70$ shows a very strong effect of polydispersity on R ; the liquid is no longer RS for polydispersities above $\delta \approx 30\%$. For $T = 1.00$, the liquid becomes non-RS at $\delta \approx 40\%$, whereas all investigated state points remain RS at $T = 4.00$. The weakening of the strong virial-potential energy correlation is thus mitigated with increasing temperature. A similar conclusion is reached when simultaneously increasing density and temperature (red

curve). The crystal state points display only a weak effect of polydispersity on R (blue curve).

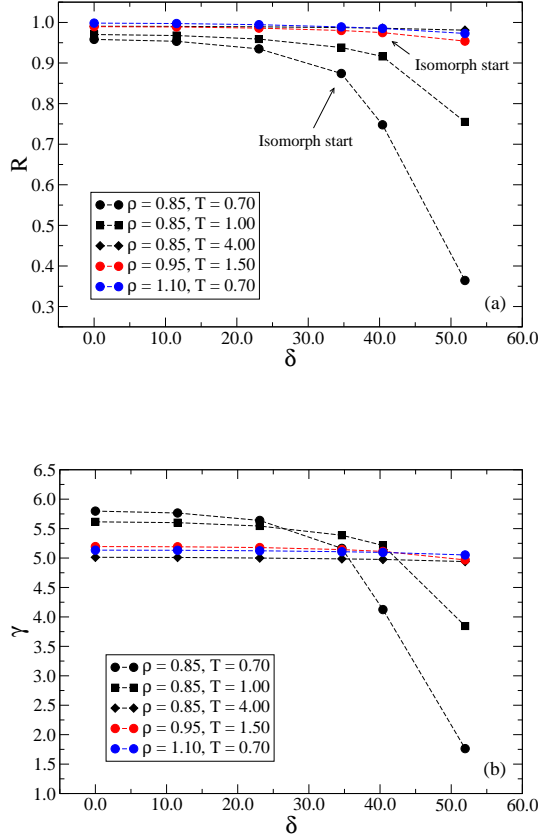


FIG. 2: Effect of polydispersity δ on the correlation coefficient R (Eq. (6)) and density-scaling exponent $\gamma \equiv \langle \Delta U \Delta W \rangle / \langle (\Delta U)^2 \rangle$ for the energy polydisperse LJ system (Eq. (2)). The paths studied are described in the text. The text “Isomorph start” refers to Sec. IV B. (a) R as function of δ . (b) γ as function of δ .

To obtain a better understanding of why R decreases so dramatically as function of polydispersity, we show in Fig. 3 a snapshot of a configuration at $\rho = 0.85$, $T = 0.70$, and $\delta = 51.96\%$ (A system with $N = 5000$ is used for illustration). Figure 3 shows that the particles are segregated to a great extent leading to the loss of the strong virial-potential energy correlation. This observation is consistent with previous investigations of the phase behavior of energy polydisperse LJ systems^{41–43}.

The particle segregation is driven by the inclusion of high ϵ_i -value particles, and can naturally be mitigated by increasing temperature and/or density and thus also explains the observed behavior for R as function of temperature and/or density (black and red curves). The particles of high ϵ_i -values crystallize after simulating the system many millions of time steps.

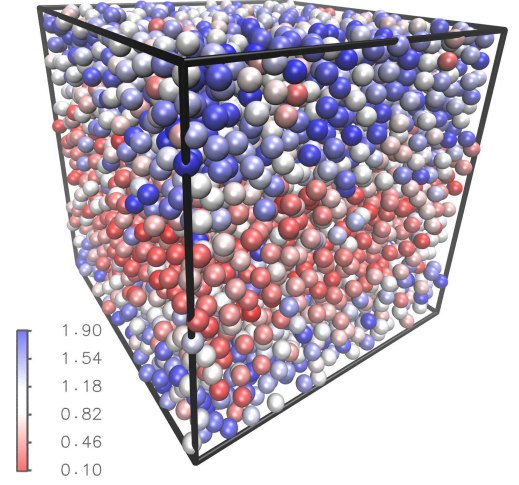


FIG. 3: Snapshot of a configuration at $\rho = 0.85$, $T = 0.70$, and $\delta = 51.96\%$ (A system with $N = 5000$ is used for illustration). Particles are colored according to their ϵ_i -values ($\epsilon_i^{\min} = 0.1$ and $\epsilon_i^{\max} = 1.9$). Phase separation is observed. The particles of high ϵ_i -values crystallize after simulating the system many millions of time steps.

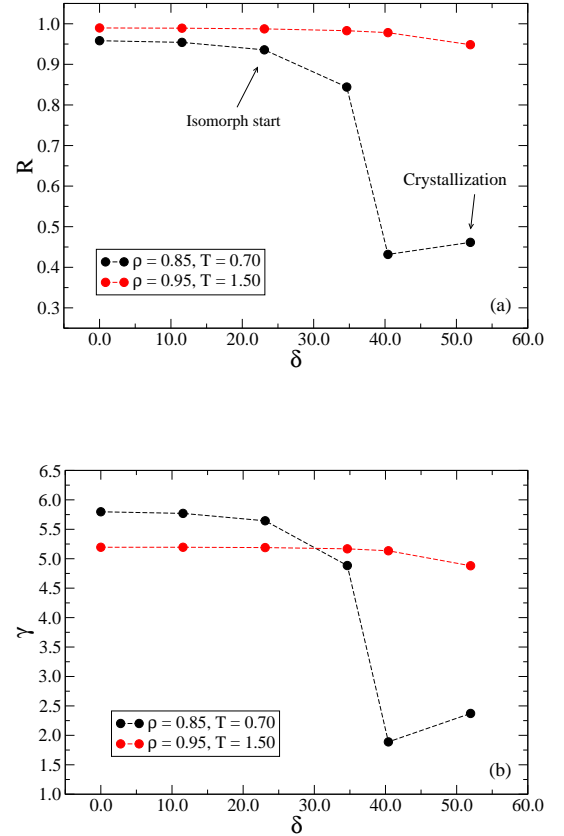


FIG. 4: Effect of polydispersity δ on the correlation coefficient R (Eq. (6)) and density-scaling exponent $\gamma \equiv \langle \Delta U \Delta W \rangle / \langle (\Delta U)^2 \rangle$ for the modified energy polydisperse LJ system (Eqs. (4) and (5)). The text “Isomorph start” refers to Sec. IV B. (a) R as function of δ . (b) γ as function of δ .

Next, Fig. 4 shows the correlation coefficient R and density-scaling exponent γ along two paths (see previous description) for the modified energy polydisperse LJ system (Eqs. (4) and (5)). Up until a polydispersity of $\delta \approx 30\%$ (black curve) R shows almost identical behavior with the original system (Fig. 2(a)). However, after passing this value the correlation coefficient drops quickly for the modified system and crystallization occurs at $\delta = 52\%$ in the simulation time scale. The density-scaling exponent γ shows a similar behavior as for the correlation coefficient. For the red curves only minor differences are noted between the two systems. The main differences between the original and modified LJ system thus first seem to appear when the original system becomes non-RS.

We believe that the difference in phase behavior between the two systems originates from the polydispersity of the repulsive core size: For the potential given by Eq. (2), energy polydispersity automatically leads to a size polydispersity of the repulsive core (see Fig. 1(a)) which causes geometrical and structural frustration against crystallization²⁸. On the other hand, for the potential given by Eqs. (4) and (5) energy polydispersity does not induce such a size polydispersity.

B. Isomorphs

Next we focus on isomorphs of energy polydisperse LJ liquids. The generation of isomorphs follows a procedure similar to that outlined in Ref. 30 by keeping $h(\rho)/T$ constant (see also Sec. III). The function $h(\rho)$ is given by^{57,63}

$$h(\tilde{\rho}) = (\gamma_*/2 - 1)\tilde{\rho}^4 + (2 - \gamma_*/2)\tilde{\rho}^2, \quad (11)$$

where $\tilde{\rho} \equiv \rho/\rho_*$, ρ_* is a chosen reference density, and γ_* is the value of $\gamma = \langle \Delta U \Delta W \rangle / \langle (\Delta U)^2 \rangle$ obtained from the equilibrium fluctuations at ρ_* (and T_*). The procedure is as follows:

1. A starting state point is chosen.
2. Density is varied by some percentage.
3. The temperature of the isomorphic state point is calculated from Eq. (11) by keeping $h(\tilde{\rho})/T$ constant.
4. A simulation is performed at the predicted state point. The procedure is then repeated by varying the density by another percentage, i.e., step 2.

Here and in the following we choose the reference density ρ_* of Eq. (11) to be that of the starting state point for the investigated isomorph⁵⁷. We start the investigation by considering an isomorph for an energy polydisperse LJ liquid (Eq. (2)) with polydispersity $\delta = 34.64\%$. The starting state point is $\rho = 0.85$ and $T = 0.70$, and has $R \approx 0.87$ (see text in Fig. 2(a)). Although the starting

state point is then a border-line RS liquid, this study can provide valuable insight into the extent to which particle segregation is isomorph invariant (see also Sec. IV A).

Radial distribution functions (RDFs) along the generated isomorph and an isotherm are displayed in Fig. 5. The isotherm serves the purpose of a reference system, as the isomorph theory is approximate^{32,35}. The average structure is to a good approximation invariant along the isomorph, but not on the isotherm where the liquid actually crystallizes.

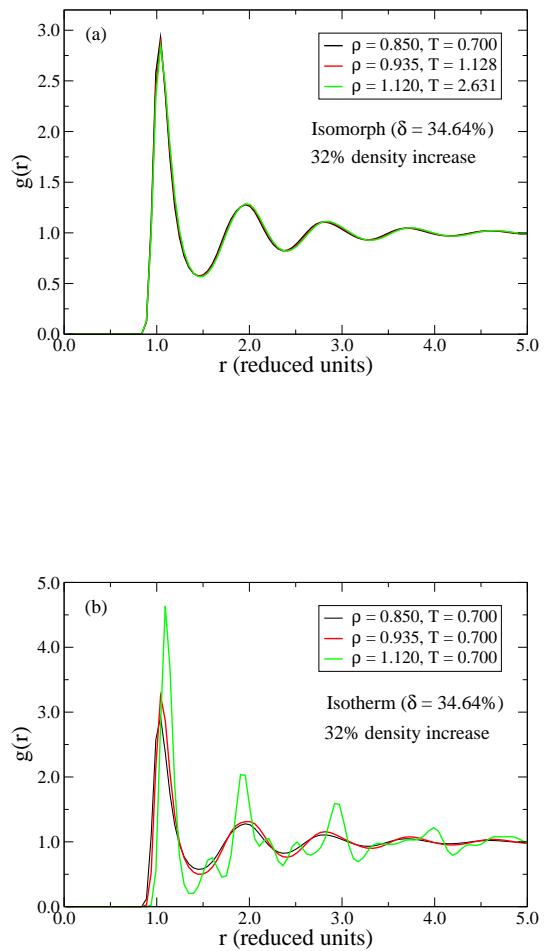


FIG. 5: Radial distribution functions (RDFs) for an energy polydisperse LJ liquid at $\delta = 34.64\%$ (Eq. (2)). (a) Along an isomorph. (b) Along an isotherm.

The dynamics for the same isomorph and isotherm is presented in Fig. 6. The mean-square displacements (MSDs) scale excellently along the isomorph, whereas the isotherm shows more than six orders-of-magnitude variation (Fig. 6(b)).

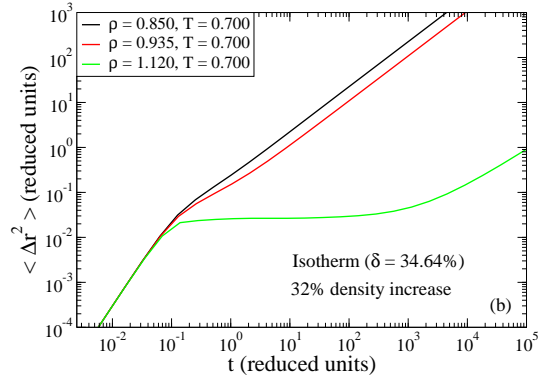
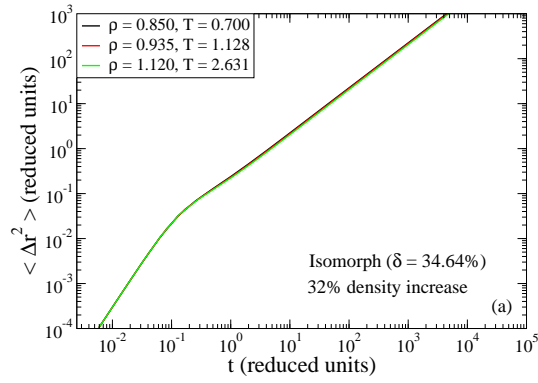


FIG. 6: Mean-square displacements (MSDs) for the energy polydisperse LJ liquid of Fig. 5. (a) Along the isomorph. (b) Along the isotherm. At the highest density (green curve) the isotherm crystallizes and gives rise to the very slow dynamics.

Particle segregation is studied in Fig. 7 by probing the static structure factor (SSF) along the same isomorph and isotherm. The low q -values of the SSF display a poor invariance along the isomorph and indicate that the particle segregation is not fully isomorph invariant. The latter is expected as the particle segregation is the reason why R decreases with increasing polydispersity (see Sec. IV A). The invariance along the isomorph is, however, much better than along the isotherm (Fig. 7(b)).

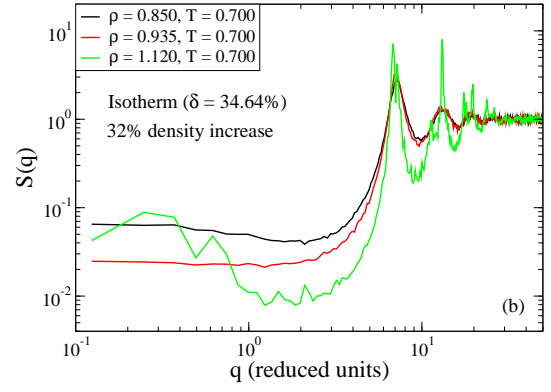
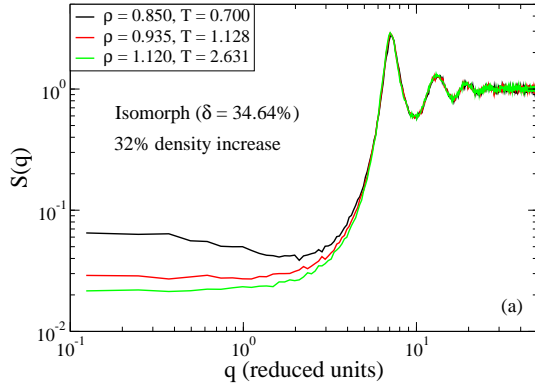
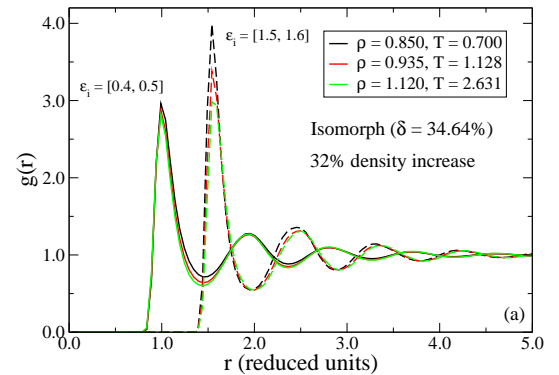


FIG. 7: Static structure factors (SSFs) for the energy polydisperse LJ liquid of Figs. 5-6. (a) Along the isomorph. (b) Along the isotherm.

The fact that the particle segregation is not isomorph invariant can also be seen by probing particle-resolved quantities. Particle-resolved RDFs are shown in Fig. 8 where the dashed curves for clarity have been shifted with 0.5 in the x -direction. The RDFs of the low ϵ_i -value particles scale well along the isomorph (full curves), but the RDFs of the high ϵ_i -value particles scale poorly (dashed curves). In both cases, however, much better than along the isotherm (Fig. 8(b)).



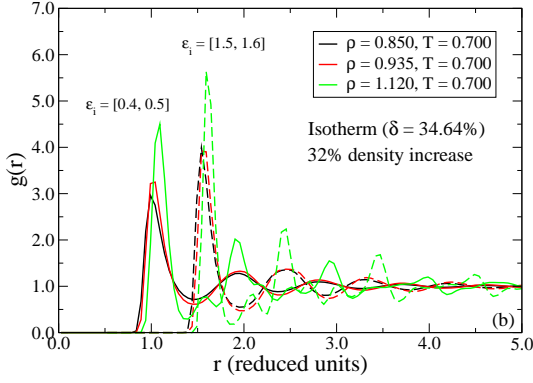


FIG. 8: Particle-resolved RDFs for the energy polydisperse LJ liquid of Figs. 5-7. The full curves use particle energies in the range $\epsilon_i = [0.4, 0.5]$, and the dashed curves use $\epsilon_i = [1.5, 1.6]$. The dashed curves have for clarity been shifted with 0.5 in the x -direction. (a) Along the isomorph. (b) Along the isotherm.

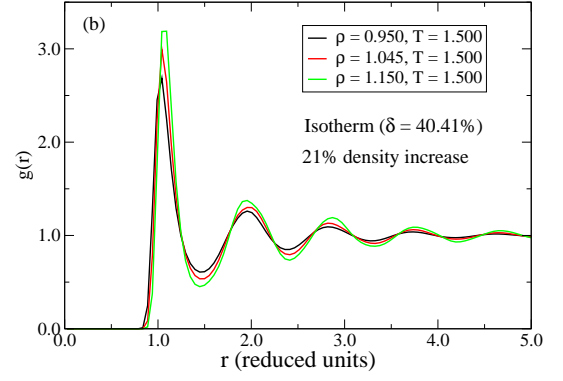


FIG. 9: RDFs for an energy polydisperse LJ liquid at $\delta = 40.41\%$ (Eq. (2)). (a) Along an isomorph. (b) Along an isotherm.

MSDs are displayed in Fig. 10 and show perfect scaling along the isomorph but not along the isotherm, as expected.

The study is now focused on an isomorph for which the energy polydispersity is very high, i.e., $\delta = 40.41\%$ (Eq. (2)). The motivation for studying such a high polydispersity is to carefully test the range of validity of isomorphs. The starting state point is $\rho = 0.95$ and $T = 1.50$ and has $R \approx 0.97$. Figure 9 displays RDFs along the isomorph and an isotherm. The RDFs scale excellently along the isomorph whereas the isotherm shows deviations; at the highest density due to crystallization during the simulation.

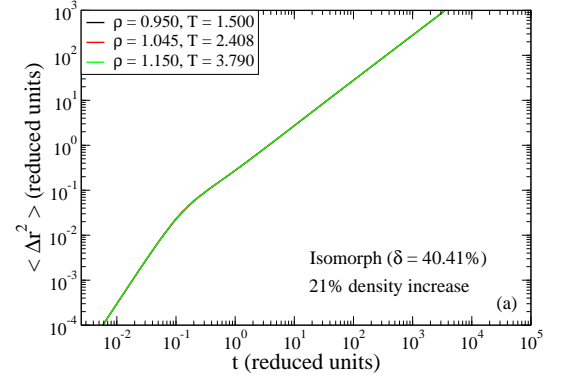
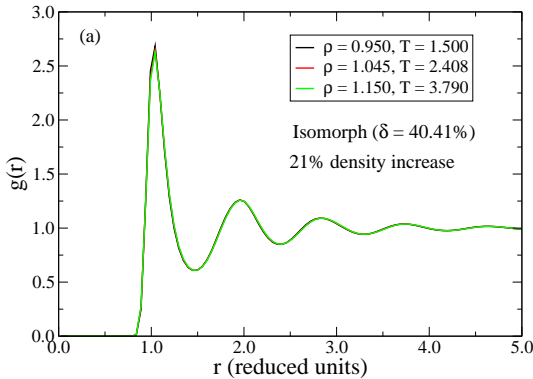


FIG. 10: MSDs for the energy polydisperse LJ liquid of Fig. 9. (a) Along the isomorph. (b) Along the isotherm.

Figure 11 presents SSFs along the same isomorph and isotherm. The isomorph displays again deviations in the low- q part of the SSF. In this case, however, much smaller deviations than the previous isomorph

as the starting state point of the isomorph has only weak particle segregation. The isotherm, on the other hand, shows very clear deviations, in particular due to crystallization.

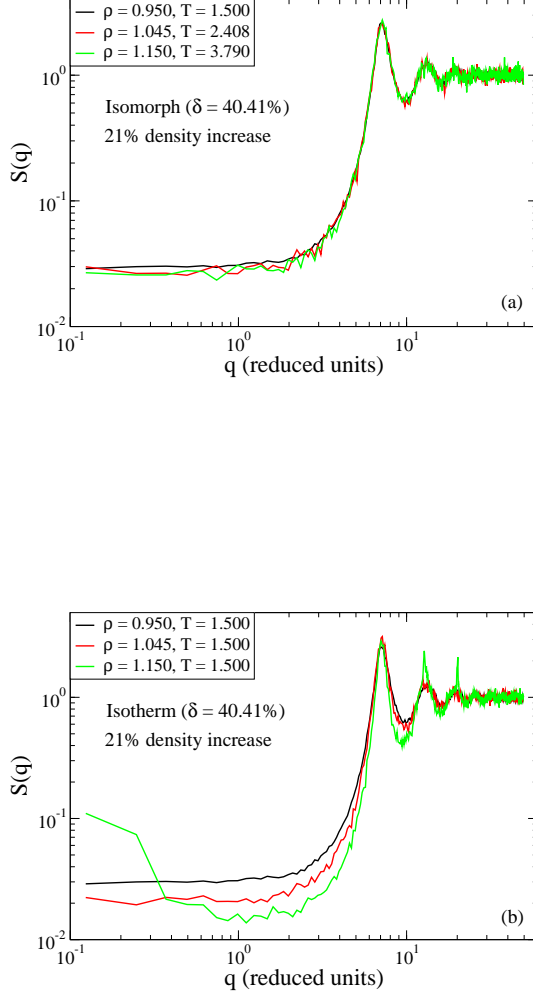


FIG. 11: SSFs for the energy polydisperse LJ liquid of Figs. 9-10. (a) Along the isomorph. (b) Along the isotherm.

Particle-resolved RDFs are presented in Fig. 12. The low and mean ϵ_i -value RDFs display good scaling along the isomorph (full and dotted curves), but the highest ϵ_i -value RDFs exhibit small deviations (dashed curves). These deviations are attributed to the non-invariant phase separation.

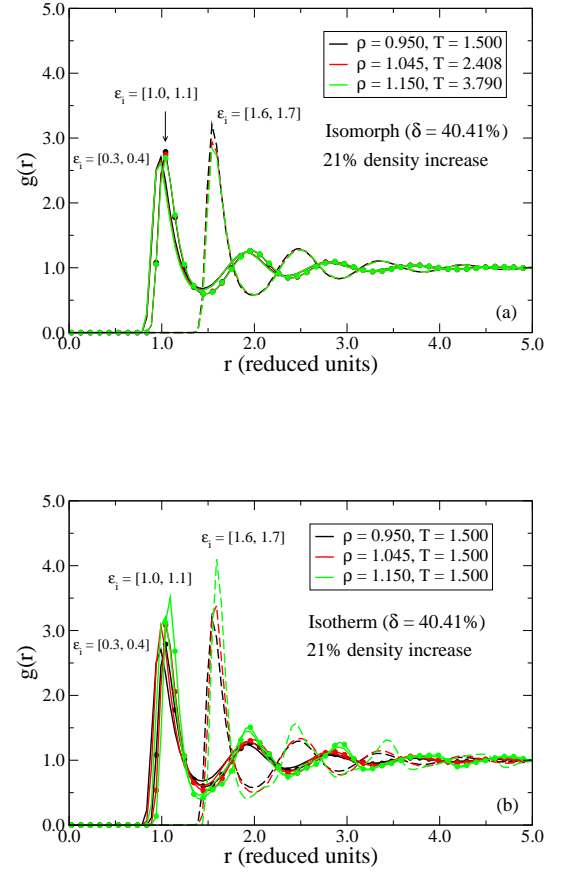
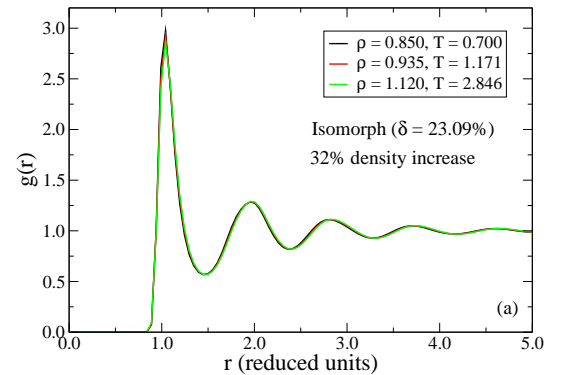


FIG. 12: Particle-resolved RDFs for the energy polydisperse LJ liquid of Figs. 9-11. The full curves use particle energies in the range $\epsilon_i = [0.3, 0.4]$, the dotted curves use $\epsilon_i = [1.0, 1.1]$, and the dashed curves use $\epsilon_i = [1.6, 1.7]$. The dashed curves have for clarity been shifted with 0.5 in the x -direction. (a) Along the isomorph. (b) Along the isotherm.

The final isomorph considered in this study is an isomorph ($R \approx 0.94$) for the modified energy polydisperse LJ system (Eqs. (4) and (5)). Figure 13 presents RDFs and MSDs along the isomorph where perfect scaling is observed.



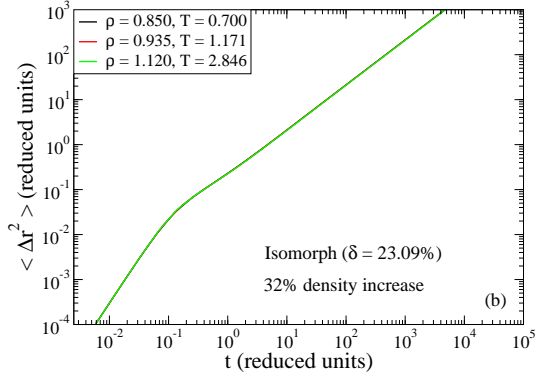


FIG. 13: Invariance along an isomorph for the modified energy polydisperse LJ system (Eqs. (4) and (5)) with $\delta = 23.09\%$. (a) RDFs. (b) MSDs.

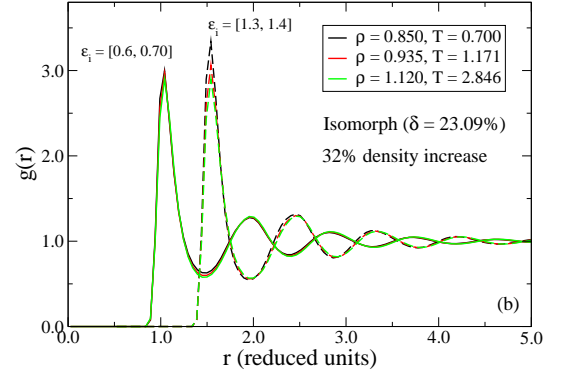


FIG. 14: Invariance along the isomorph of Fig. 13 for the modified energy polydisperse LJ system with $\delta = 23.09\%$. (a) SSFs. (b) Particle-resolved RDFs. The full curves use particle energies in the range $\epsilon_i = [0.6, 0.7]$, and the dashed curves use $\epsilon_i = [1.3, 1.4]$. The dashed curves have for clarity been shifted with 0.5 in the x -direction.

Figure 14 displays SSFs and particle-resolved RDFs along the same isomorph. The SSF and large ϵ_i -particles are again noted to exhibit deviations along the isomorph for this moderately polydisperse system ($\delta = 23.09\%$), and is ascribed to the phase separation as is evident from Fig. 14(a).

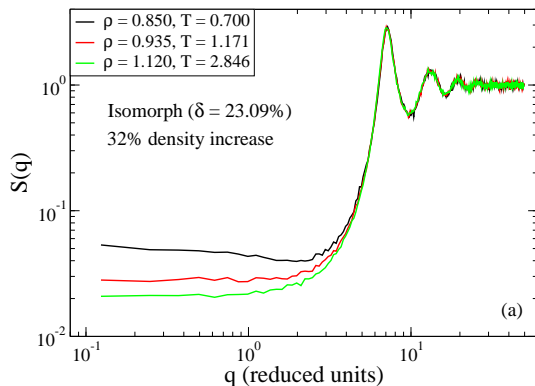
V. CONCLUSION AND OUTLOOK

Polydisperse fluids are interesting to theoreticians and experimentalists alike owing to the perplexing phenomena these fluids display. In the companion paper³⁰ we studied the effect of size polydispersity on the nature of LJ liquids. The paper showed that even highly size polydisperse LJ liquids are RS liquids³². Furthermore, it was shown that isomorphs extend readily to size polydisperse LJ liquids.

We considered in this paper the effect of energy polydispersity on the nature of LJ liquids. It was shown that highly energy polydisperse LJ liquids are also RS liquids. Particle segregation, however, leads to the loss of strong virial-potential energy correlation as a function of polydispersity. Depending on the investigated state point, this effect influences the strong virial-potential energy correlation to the extent that the liquid turns into a non-RS liquid.

This decrease of the strong virial-potential energy correlation is a consequence of the fact that energy polydispersity leads to a serious modification of the phase behavior (see Fig. 3). In comparison, for size polydisperse systems, the effects on the phase behavior are much weaker³⁰. Isomorphs of energy polydisperse LJ liquids were also studied and shown to be a good approximation. Nevertheless, particle-resolved quantities showed larger deviations than the mean quantities along the isomorph due to the phase separation. This observation may thus affect particle-resolved scaling relations in polydisperse fluids⁶⁴.

Motivation for the current study is derived from the fact that experimental polydisperse liquids are often dispersed in additional variables besides their size. As an example: Colloidal fluids can have a distribution in their size as well as their charge. Energy polydisperse liquids are less experimentally realizable than size polydisperse



liquids. We believe, however, that the insight gained from this kind of study is imperative for understanding the effect of polydispersity on the nature of LJ liquids.

Size and energy polydisperse LJ liquids are both RS liquids, however, the extent to which depends strongly on the type of polydispersity. Additional studies of polydispersity in relation to strong virial-potential energy correlation are thus needed to fully understand the effect of polydispersity on more complex RS liquids. The Yukawa potential was recently identified as RS in large parts of its phase diagram⁶⁵. It would be interesting to study a polydisperse version of this system and also of high relevance to experiments. We plan to address these issues

in a later publication, and also welcome other studies of polydispersity and RS liquids.

Acknowledgments

This work was partially supported by Grants-in-Aid for Scientific Research (S) (21224011) and Specially Promoted Research (25000002) from the Japan Society of the Promotion of Science (JSPS). T.S.I. acknowledges support from a JSPS Postdoctoral Fellowship.

-
- * Electronic address: trond@iis.u-tokyo.ac.jp
† Electronic address: tanaka@iis.u-tokyo.ac.jp
- ¹ B. Bagchi, *Molecular Relaxation in Liquids* (Oxford University Press: New York, 2012).
 - ² P. G. Wolynes and V. Lubchenko, eds., *Structural Glasses and Supercooled Liquids: Theory, Experiment, and Applications* (John Wiley and Sons, Inc.: New Jersey, 2012).
 - ³ J. S. Hansen, C. A. Lemarchand, E. Nielsen, J. C. Dyre, and T. Schröder, *J. Chem. Phys.* **138**, 094508 (2013).
 - ⁴ E. Dickinson, *Chem. Phys. Lett.* **57**, 148 (1978).
 - ⁵ L. Blum and G. Stell, *J. Chem. Phys.* **71**, 42 (1979).
 - ⁶ J. J. Salacuse and G. Stell, *J. Chem. Phys.* **77**, 3714 (1982).
 - ⁷ M. Ginoza and M. Yasutomi, *Mol. Phys.* **91**, 59 (1997).
 - ⁸ P. Sollich, *J. Phys.: Condens. Matter* **14**, R79 (2002).
 - ⁹ M. Fasolo and P. Sollich, *Phys. Rev. Lett.* **91**, 068301 (2003).
 - ¹⁰ W. M. Jacobs and D. Frenkel, *J. Chem. Phys.* **139**, 024108 (2013).
 - ¹¹ D. Frenkel, R. J. Vos, C. G. de Kruif, and A. Vrij, *J. Chem. Phys.* **84**, 4625 (1986).
 - ¹² D. A. Kofke and E. D. Glandt, *FFE* **29**, 327 (1986).
 - ¹³ N. B. Wilding and P. Sollich, *J. Phys.: Condens. Matter* **17**, S3245 (2005).
 - ¹⁴ N. B. Wilding, P. Sollich, and M. Fasolo, *Phys. Rev. Lett.* **95**, 155701 (2005).
 - ¹⁵ N. B. Wilding, P. Sollich, M. Fasolo, and M. Buzzacchi, *J. Chem. Phys.* **125**, 014908 (2006).
 - ¹⁶ T. Kawasaki, T. Araki, and H. Tanaka, *Phys. Rev. Lett.* **99**, 215701 (2007).
 - ¹⁷ S. Sarkar, R. Biswas, M. Santra, and B. Bagchi, *Phys. Rev. E* **88**, 022104 (2013).
 - ¹⁸ S. Sarkar, R. Biswas, P. P. Ray, and B. Bagchi, arXiv p. 1402.6879 (2014).
 - ¹⁹ R. Koningsveld and L. A. Kleintjens, *Macromolecules* **4**, 637 (1971).
 - ²⁰ C. Cowell and B. Vincent, *J. Colloid Interface Sci.* **87**, 518 (1982).
 - ²¹ E. R. Weeks, J. C. Crocker, A. C. Levitt, A. Schofield, and D. A. Weitz, *Science* **287**, 627 (2000).
 - ²² S. Auer and D. Frenkel, *Nature* **413**, 711 (2001).
 - ²³ K. Watanabe and H. Tanaka, *Phys. Rev. Lett.* **100**, 158002 (2008).
 - ²⁴ S. Sacanna, M. Korpics, K. Rodriguez, L. Colón-Meléndez, S.-H. Kim, D. J. Pine, and G.-R. Yi, *Nat. Commun.* **4**, 1688 (2013).
 - ²⁵ T. Palberg, *J. Phys.: Condens. Matter* **26**, 333101 (2014).
 - ²⁶ M. Leocmach and H. Tanaka, *Nat. Commun.* **3**, 974 (2012).
 - ²⁷ H. Tanaka, *Eur. Phys. J E* **35**, 113 (2012).
 - ²⁸ M. Leocmach, J. Russo, and H. Tanaka, *J. Chem. Phys.* **138**, 12A536 (2013).
 - ²⁹ R. M. L. Evans, *Phys. Rev. E* **59**, 3192 (1999).
 - ³⁰ T. S. Ingebrigtsen and H. Tanaka, *J. Phys. Chem. B* **119**, 11052 (2015).
 - ³¹ U. R. Pedersen, N. P. Bailey, T. B. Schröder, and J. C. Dyre, *Phys. Rev. Lett.* **100**, 015701 (2008).
 - ³² N. P. Bailey, U. R. Pedersen, N. Gnan, T. B. Schröder, and J. C. Dyre, *J. Chem. Phys.* **129**, 184507 (2008).
 - ³³ N. P. Bailey, U. R. Pedersen, N. Gnan, T. B. Schröder, and J. C. Dyre, *J. Chem. Phys.* **129**, 184508 (2008).
 - ³⁴ T. B. Schröder, N. P. Bailey, U. R. Pedersen, N. Gnan, and J. C. Dyre, *J. Chem. Phys.* **131**, 234503 (2009).
 - ³⁵ N. Gnan, T. B. Schröder, U. R. Pedersen, N. P. Bailey, and J. C. Dyre, *J. Chem. Phys.* **131**, 234504 (2009).
 - ³⁶ T. B. Schröder, N. Gnan, U. R. Pedersen, N. P. Bailey, and J. C. Dyre, *J. Chem. Phys.* **134**, 164505 (2011).
 - ³⁷ T. S. Ingebrigtsen, T. B. Schröder, and J. C. Dyre, *Phys. Rev. X* **2**, 011011 (2012).
 - ³⁸ T. S. Ingebrigtsen, T. B. Schröder, and J. C. Dyre, *J. Phys. Chem. B* **116**, 1018 (2012).
 - ³⁹ J. Largo and N. B. Wilding, *Phys. Rev. E* **73**, 036115 (2006).
 - ⁴⁰ M. R. Stapleton, D. J. Tildesley, T. J. Sluckin, and Q. N., *J. Phys. Chem.* **92**, 4788 (1988).
 - ⁴¹ L. S. Shagolsem, D. Osmanović, O. Peleg, and Y. Rabin, *J. Chem. Phys.* **142**, 051104 (2015).
 - ⁴² L. S. Shagolsem and Y. Rabin, arXiv p. 1508.05264v1 (2015).
 - ⁴³ D. Osmanović and Y. Rabin, *J. Stat. Phys.* **162**, 186 (2016).
 - ⁴⁴ S. Toxvaerd, *Mol. Phys.* **72**, 159 (1991).
 - ⁴⁵ N. P. Bailey, T. S. Ingebrigtsen, J. S. Hansen, A. A. Veldhorst, L. Bøhling, C. A. Lemarchand, A. E. Olsen, A. K. Bacher, H. Larsen, J. C. Dyre, et al., arXiv p. 1506.05094 (2015).
 - ⁴⁶ M. P. Allen and D. J. Tildesley, *Computer Simulation of Liquids* (Oxford University Press: New York, 1987).
 - ⁴⁷ J. C. Dyre, *J. Phys. Chem. B* **118**, 10007 (2014).
 - ⁴⁸ D. E. Albrechtsen, A. E. Olsen, U. R. Pedersen, T. B. Schröder, and J. C. Dyre, *Phys. Rev. B* **90**, 094106 (2014).
 - ⁴⁹ D. Coslovich and C. M. Roland, *J. Phys. Chem. B* **112**,

- 1329 (2008).
- ⁵⁰ D. Coslovich and C. M. Roland, *J. Chem. Phys.* **130**, 014508 (2009).
 - ⁵¹ T. B. Schröder, U. R. Pedersen, N. P. Bailey, S. Toxvaerd, and J. C. Dyre, *Phys. Rev. E* **80**, 041502 (2009).
 - ⁵² W. Kob and H. C. Andersen, *Phys. Rev. E* **51**, 4626 (1995).
 - ⁵³ L. J. Lewis and G. Wahnström, *J. Non-Cryst. Solids* **172-174**, 69 (1994).
 - ⁵⁴ D. Gundermann, U. R. Pedersen, T. Hecksher, N. P. Bailey, B. Jakobsen, T. Christensen, N. B. Olsen, T. B. Schröder, D. Fragiadakis, R. Casalini, et al., *Nat. Phys.* **7**, 816 (2011).
 - ⁵⁵ L. A. Roed, D. Gundermann, J. C. Dyre, and K. Niss, *J. Chem. Phys.* **139**, 101101 (2013).
 - ⁵⁶ W. Xiao, J. Tofteskov, T. V. Christensen, J. C. Dyre, and K. Niss, *J. Non-Crystal. Solids* **407**, 190 (2015).
 - ⁵⁷ T. S. Ingebrigtsen, L. Bøhling, T. B. Schröder, and J. C. Dyre, *J. Chem. Phys.* **136**, 061102 (2012).
 - ⁵⁸ T. S. Ingebrigtsen, J. R. Errington, T. M. Truskett, and J. C. Dyre, *Phys. Rev. Lett.* **111**, 235901 (2013).
 - ⁵⁹ T. S. Ingebrigtsen and J. C. Dyre, *Soft Matter* **10**, 4324 (2014).
 - ⁶⁰ L. Separdar, N. P. Bailey, T. B. Schröder, S. Davatolhagh, and J. C. Dyre, *J. Chem. Phys.* **138**, 154505 (2013).
 - ⁶¹ A. A. Veldhorst, J. C. Dyre, and T. B. Schröder, *J. Chem. Phys.* **141**, 054904 (2014).
 - ⁶² T. B. Schröder and J. C. Dyre, *J. Chem. Phys.* **141**, 204502 (2014).
 - ⁶³ L. Bøhling, T. S. Ingebrigtsen, A. Grzybowski, M. Paluch, J. C. Dyre, and T. B. Schröder, *New J. Phys.* **14**, 113035 (2012).
 - ⁶⁴ M. J. Pond, J. R. Errington, and T. M. Truskett, *J. Chem. Phys.* **135**, 124513 (2011).
 - ⁶⁵ A. A. Veldhorst, T. B. Schröder, and J. C. Dyre, *Phys. Plasmas* **22**, 073705 (2015).